

Machine Learning Enabled Large-Scale Estimation of Residential Wall Thermal Resistance from Exterior Thermal Imaging

Salahaldin F. Alshatshati*, Kevin P. Hallinan, Rodwan Elhashmi and Kefan Huang
Department of Mechanical and Aerospace Engineering University of Dayton, Dayton, OH
*Corresponding Author's Email: alshatshatis1@udayton.edu

Abstract— Traditional building energy audits are both expensive, in the range of USD\$1.29/m²-USD\$5.37/m², and inconsistent in their prediction of potential energy savings. Automation to reduce costs of evaluating the energy effectiveness of buildings is strongly needed. A key element of such automation is a means to estimate the building envelope energy effectiveness. We present a method that addresses this need by using infrared thermography to characterize building wall envelope effectiveness. To date, thermal imaging approaches for estimating wall R-Values, based upon thermal-physical models of walls, require additional manual measurements and analysis which prohibit low-cost, large-scale implementation. To overcome this implementation challenge, a machine learning approach is used to predict wall R-Values for a set of residences with known thermal resistance by utilizing the measured wall imaging temperature, prior weather conditions, historical energy consumption data, and available building geometrical data. The developed model is shown to predict wall R-Values with a maximum test-set root mean squared error of 7% using as few as nine training houses. This result has significant implications for low-cost large-scale envelope energy effectiveness characterization.

Keywords— Thermal Imaging, Wall Thermal Resistance, Machine Learning, energy audits

I. INTRODUCTION

A comprehensive study published in 2015 shows that there are about 5.6 million commercial buildings in the U.S., most of which were constructed before 1980 [1]. A 2003 survey by the U.S. EIA suggested that 75% of commercial buildings that were built prior to 1960 did not have insulation upgrades [2]. Similarly, a 2001 U.S. EIA report documented that only 40.3% of U.S. residences were considered well insulated, while more than 20% were poorly insulated or not insulated at all [3]. Finally, a recent study, based on a one-factor-at-a-time evaluation of building enclosure measures, estimated that wall insulation upgrades to R30 (5.3 K·m²/W) across the spectrum of buildings present in the mid-Atlantic region could result in a 17.1% reduction in total energy consumption [4]. Extending this result to the U.S. as a whole gives savings estimates for cooling and heating of respectively 0.0875 and 0.506 EJ.

Buildings which already have well-insulated envelopes offer little savings benefit, and therefore a major challenge is the identification of buildings which have the greatest need for weatherization upgrades. However, this prioritization is laborious, requiring a large number of manual energy audits at a minimum. A comprehensive set of audits would not only be expensive, but also far exceed the capacity of the existing

number of auditors available [5]. State of the art energy auditing costs up to \$5.38/square meter [6]. Given a total U.S. building floor area of approximately 32.7 billion square meters, the cost to audit the entire building U.S. building stock would be in the range of USD\$42-175 billion [1].

Utility analysis has proven effective for identifying buildings with high energy consumption and verifying savings from retrofits at scale [7]. The basic idea in utility analysis is to correlate energy consumption with external temperature and other factors. For temperature-only considerations, linear regressions have been used to estimate energy consumption sensitivity to weather. These sensitivities, when applied to typical weather years, have permitted estimates of weather normalized energy consumption [8] [9].

Increasingly sophisticated machine learning applied to these data have rendered an increasing amount of information about the energy effectiveness of buildings [10]; [11]. For example, a recent study by [12] used an expanded set of residential building energy characteristics that included wall, window, and roof R-Values, coupled with energy consumption data, to predict savings from the adoption of individual measures. This approach was based strictly on actual building data, not on physics-based energy models, and the demonstrated results indicated that predicted annual savings from HVAC related upgrades matched within 2.5 percent of realized savings for most of the measures considered. Critical to Atarhuni et al.'s study was the use of a large number of buildings/residences for which the most important energy characteristics were known.

Large scale (i.e., at the scale of a utility district) thermal imaging of building envelopes could be a component of this type of audit to quantify envelope R-Values. The efficacy of using these thermal images at such a scale has been demonstrated [13]; [14], but inferring R-Values in an easily automated way remains an open challenge.

Extracting R-Value estimates from infrared thermal imaging has been limited by uncertainties that include an inaccurate accounting or a neglect of the influence of wind on convection heat transfer on exterior surfaces, a lack of knowledge of the interior temperature, inaccurate specification of the infrared spectrum exterior surface emissivity, inaccurate specification or neglect of background radiation rendering reflection from the imaged surfaces, and a neglect of dynamic effects arising from transient weather conditions or variable internal temperature schedules.

A number of researchers have added measurements coincidental with the infrared thermography of the surface to the analysis used to extract the R-Values. The error in estimating the R-Value associated with the exterior convection coefficient has been addressed by measuring the wind speed near or very near the surface being imaged [15], [16], [17], [18], [19], [20]. The error arising from uncertainty in knowing the internal temperature has been overcome by direct measurement [18], [21], [22], [23], from exterior thermal imaging through a partially opened window [15], [16], [17], [19], and [20], and through connection to a Building Information Management (BIM) system [24]. In order to reduce the exterior surface emissivity specification error which renders error in inferring the surface temperature from the thermal image, researchers have either added targets with known emissivities to or near the surface being thermally imaged [15], [16], [19], [20], thermally imaged an unheated/uncooled surface with identical surface finish as the targeted surface for thermal imaging [25], or measured the surface emissivity with an emissometer [17]. The error associated with incorrect specification of or neglect of reflected energy from the surface has been overcome through the use of reflective targets applied to the imaged surfaces [18], [21], [25], [19], [20]. Last of all the errors associated with neglecting dynamic influences on the surface temperature have been addressed by restricting the use of thermography to near steady weather conditions [15], [16], [17], [18], [21], [19], [20], through multiple measurements taken at different times and seasons or through continuous monitoring over a relatively short period of time [25], [26], and through integration of the thermography inferred exterior surface temperature into a dynamic thermal building model [22], [23]. Table 1 summarizes this review.

Collectively these approaches have yielded excellent predictions of R-Values. For example, Madding (2008) reported errors in predicting the R-Value between 5-12% [27]. Fokaides and Kalogirou (2011) report errors in the range of 10-20% [21]. Dall'O et al. (2013) report R-Value errors as high as 50% for well-insulated walls associated with the high R-value walls where the temperature difference between the exterior wall and ambient environment is small [25]. Nardi et al. (2014) reported errors in the range of 1-12% [19]. However, the primary weakness of these approaches is the time required to analyze collected data. Any of the processes that require placement of additional targets, either reflective or of known emissivity, virtually negate potential low cost, at-scale implementation. The same could be said about the use of anemometry measurement of the wind speed near the surface. Further, development of a 3D dynamic house model [22], [23] using IR obtained exterior wall temperatures as input would be impossible to do with low cost and at-scale [22], [23].

Recognizing both the promise of automated energy audits in identifying priority energy savings at regional and national scales, we propose a method to predict residential wall R-Values from exterior infrared thermal imaging in a way that preserves current accuracy levels and critically, can be implemented at large scales and at low cost. The approach posed requires no additional measurement other than thermography. Instead it leverages additional data about each residence, including publicly accessible building geometry information, local

historical weather data, and historical energy data. We combine this information with known wall R-Values obtained from residential audits in order to develop a data-based model capable of accurate prediction of wall R-Values in residence where audits have not been performed.

Table 1: Summary of measurements/approaches made by prior researchers to reduce error in estimating the wall R-Value from building envelopes

Authors	Wind speed near surface	Interior Temperature	Targets to capture geometry	Mean reflective temperature	Knowing emissivity targets	Ambient Temperature	Dynamic Effects	Multiple measurement times
Albatici & Tonelli, 2008 [15], Albatici & Tonelli, 2010 [16]								
Grinzato et al. 2010 [18]								
Fokaides & Kalogirou, 2011 [21]								
Dall'O et al. 2013 [25]								
Ham & Golparvar-Fard, 2013 [22]								
Nardi et al. 2014 [19]								
Ham & Golparvar-Fard, 2014 [23]								
Ham & Golparvar-Fard, 2015 [24]								
Albatici et al. 2015 [17]								
Nardi et al. 2016 [20]								

In the remainder of this manuscript, we first present the data and pre-processing steps utilized for this study, and then describe the machine learning approaches employed. Next the results are presented, including model predictive statistics and validation results. Finally, we summarize the results, discuss the practical implications of the work, and identify shortcomings and future needs

II. METHODOLOGY

A. Data Description

During the summer of 2015 energy audits were completed on a total of 142 student residential homes owned by a Midwestern US university. These audit data included a determination of the amount and type of insulation in the walls and roof, areas and types of windows, floor heights, maximum occupancy, appliance (refrigerator, range, and oven) specifications, heating ventilation air-conditioning system specifications, domestic hot water equipment specifications, the

presence of a basement, and interior house to attic penetration area. The local county database was used to obtain detailed geometrical features of each residence, including the year built, floor area for each level, number of baths, number of bedrooms, and total floor area. Historical monthly energy consumption (gas and electric) data were collected for each residence for the period from January 2014 through August 2015. From these data, some general energy characteristic trends were observed. The oldest homes, constructed in the early 1900s, generally had very little insulation in the walls and ceilings. The windows in these homes were mostly double-paned or single-paned with storm windows. Some of these houses had been recently upgraded with improved energy effective systems or demolished and replaced with newer, more energy effective residences. The renovations included double-paned window replacements and the addition of 125 mm insulating wall board to the exterior wall of the residences beneath new siding. The newest homes, by contrast, were constructed in adherence to U.S. Department of Energy Star criterion. Additionally, over time, some very old furnaces and water heaters had been replaced with high efficiency units in many of the residences.

Critical to this study is a reasonable distribution of energy characteristics among the housing set targeted. Table 2 documents the range of residential building characteristics measured among the houses audited. All walls were wood framed walls with either 2x4 or 2x6 construction. The R-Values presented in the tables represent clear ‘wall’ calculated values from knowledge of the type of construction and the amount of fiberglass insulation in the walls. All houses had vinyl or wood siding. Of these, 41 had low or medium wall R-Values and twelve had high wall R-Values. For example, the wall R-Value ranges from 0.7 to 2.43 m².K/W, the roof R-Value ranges from 1.14 to 7.04 m².K/W, and the natural gas fueled furnace efficiency ranges from 55% to 95%. For this study, a random sample comprising 53 houses of the full dataset was selected for thermal imaging.

Table 2: Residential building geometrical and energy data and range of values made during the summer 2015 audit

House characteristics	Minimum	Maximum
Attic penetration area (cm2)	0	3716
Basement vent area (cm2)	0	348
Floor area (m2)	66	258
Window area (m2)	7	27
Wall area (m2)	54	302
R-Value roof (m2.K/W)	1.14	7
R-Value windows (m2.K/W)	0.18	0.35
R-Value wall (m2.K/W)	0.70	2.43
R-Value basement (m2.K/W)	0.70	0.88
Energy factor for water heater	0.55	0.95
Furnace efficiency (%)	60%	97.4%
Number of occupants	2	12
Seasonal Energy Efficiency Ratio (SEER)(AC)	NA	16

The historical monthly energy usage for each building was combined with the known historical weather condition data for each meter period in order to develop new energy characteristics of the residence. The Prism methodology was employed to do this (Fels 1986). This approach renders a simple, pseudo-

mechanistic model for predicting monthly energy consumption, $E_{i,gas}$, of the form of:

$$E_{i,gas} = E_{baseline,gas,i} + HS_{gas}(T_{balh,gas} - T_{outside}) H(T_{balh,gas} - T_{outside}) \quad (1)$$

This equation includes three fit parameters, $E_{baseline,gas,i}$ (MJ m⁻² month⁻¹), the average monthly weather-independent natural gas energy intensity, HS_{gas} (Wm⁻² K⁻¹), the weather-sensitive monthly gas energy intensity with outdoor temperature, and the $T_{balh,gas}$ (°C), the heating balance point temperature associated with the average temperature below which heating occurs. In this equation, the function H is the Heaviside function. These fit parameters are effectively energy system characteristics of the houses. The derived slope accounts not only for losses through the walls, windows, and ceiling, but also infiltration, passive solar heat gain, plug loads, human loads, and water heating loads which translate to heating within a residence. The average monthly weather independent energy consumption, $E_{baseline,gas,i}$, accounts for the water heating energy consumption of the residence for the houses in this study. Lastly, the heating balance point temperature accounts partly for residential variation in thermostat setpoint scheduling. The most important point here is that that the weather sensitive fit parameter, HS_{gas} , accounts for the amount of wall insulation. If the wall insulation is increased, the value of this terms decreases.

The annual normalized annual heating can be determined by translating these fit values to a typical weather year, where the summation is over every hour in the year and T_i is the typical hourly temperature for a specific hour, i , in the year.

$$NAHC [MJ m^{-2} year^{-1}] = HS \sum_i^{8760} (T_{balh} - T_i) \quad (2)$$

A FLIR SC8303 thermal imaging camera was used for the imaging. All thermal images were acquired around 4 am during cold winter mornings over a one-month period to minimize the effect of solar absorption during the day. All raw images were reduced assuming a surface emissivity of 0.9. An average temperature of each surface was calculated based on this estimate. Previous research by the authors [28] demonstrated that a 5% error in estimating the emissivity could translate to a 20% error in estimating the R-Value using a dynamic model of the envelope. Thus, there was need to better estimate the emissivity of the surfaces being used. For this study, a visual approach was employed to characterize the far infrared spectral emissivity of the various surfaces imaged using the available emissivity databases [29], [30]. Ultimately, this approach could be automated using image processing. A corrected temperature for each surface was calculated using Equation (2). Use of this equation assumes that the wall surface radiosity is dominated by emitted energy from the surface, not reflected energy. Given that all walls imaged were estimated to have emissivities greater than 0.8, this assumption is reasonable.

$$T_{\text{inferred emissivity}} = T_{\text{measured at } \epsilon=0.9} \times \left(\frac{\epsilon = 0.9}{\epsilon}\right)^{0.25} \quad (3)$$

Last of all, the wind speed, exterior temperature, and solar flux for 48 hours prior to each image were acquired from an on-site weather station. A local Onset Hobo weather station located within 0.5 km of all homes imaged was used to collect this data. Data was sampled at 1-minute intervals. Thus, for each imaging event, the weather conditions prior to the imaging were available.

Ultimately the features shown in Table 3 were used to predict the wall R-Value. Each observation included the following predictors: the corrected wall temperature measurement from the infrared thermography, HS , T_{balh} , $Baseline_{gas,i}$, total floor area (A_f), wall area (A_w), attic area (A_{at}), total window area (A_{win}), heating slope (HS), and maximum occupancy (O_M). To capture the dynamic effect owing to weather transients, the ambient air temperature from two hours, five hours, and twelve hours prior to the imaging and averaged over the past 48 hours were included as predictors. In addition, the vertical solar radiation flux averaged over the past 48 hours was considered as a predictor. Finally, the target variable is the measured wall R-Value.

Table 3: Predictor variables for data-mining approach

Variable Name	Description
$T_{measured}$	Corrected wall surface temperature (K)
I_{48} , previous 48 hr (average)	Vertical solar radiation (W m-2), averaged over previous 48 hours
$T_{\infty-48}$, previous 48 hr (average)	Ambient temperature, averaged over previous 48 hours
HS	Heating intensity slope (W m-1K-1)
Tbalh	Heating balance point temperature (K)
Baseline _{gas,i}	Weather independent monthly gas intensity, (MJ month-1 m-2)
A_w/A_f	Ratio of wall to floor area
O_M	Occupancy maximum
T_{∞}	Ambient temperature at imaging time (K)
$T_{\infty-2}$	Ambient temperature two hours prior to the imaging time (K)
$T_{\infty-5}$	Ambient temperature five hours prior to the imaging time (K)
$T_{\infty-12}$	Ambient temperature twelve hours prior to the imaging time (K)

B. Data Pre-Processing

We used three primary pre-processing steps. In the first, a Pearson correlation plot (Figure 1) was developed to investigate feature correlation. This figure shows that the predictors are not highly correlated (correlation coefficient $\sim > 0.7$) to include in the model except for the ambient temperatures with respect to time. This may or may not be true in general. The second pre-processing step was to normalize all data from 0 to 1 for each predictor. To do this the mean, maximum, and minimum values of each predictor were obtained. The scaled values for each predictor then were calculated according to Equation (4) below.

$$Scaled\ predictor = \frac{predictor\ value - min\ value}{max\ value - mini\ value} \quad (4)$$

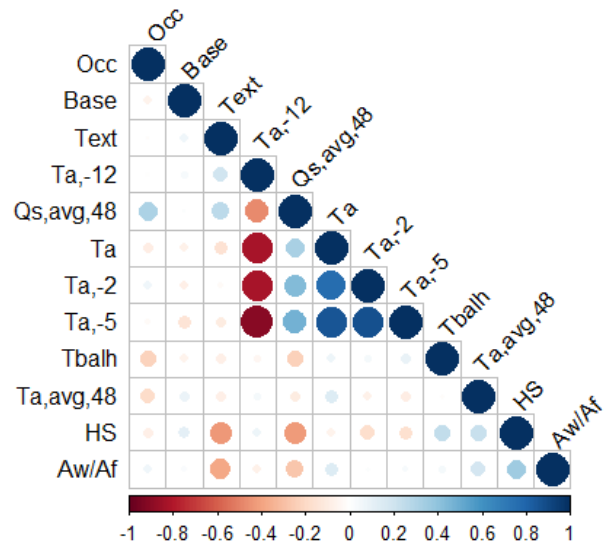


Figure 1: Pearson correlation plot for all potential predictors

We considered up-sampling the data to yield a training dataset which would have a uniform distribution in the wall R-value. However, as shown in Figure 2, there were three dominant wall R-Values, with a reasonable number of observations in each of the ‘bins’. Figure 2 shows a histogram of the scaled values of the wall R-Values of the complete dataset.

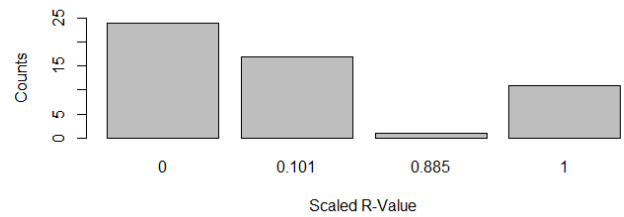


Figure 2: Histograms of scaled wall R-Value in the original data

C. Model Training Data

In order to develop machine learning models capable of predicting the wall R-Values, the wall R-Value must be known for at least a sampling of residences. Due to the expense (both in time and capital) of individual audits, it is important to purposefully select the houses to audit in order to guarantee that houses with high, medium, and low wall R-Values are in the training set used to develop the model. Two approaches are posited for identifying these training houses. The first is to group houses according to NAHC into low, medium, and high values. These houses could be audited prior to the imaging date. The second approach is to first collect and examine imaging data, and then subsequently audit select houses. In this method, the measured exterior wall temperatures from the collective group of houses imaged would be grouped into low, medium, and high

bins and then reference houses to be audited would be randomly selected from these subsets.

Figure 3a and 3b respectively show the relationship between the NAHC and corrected measured surface temperature versus the wall R-Value. Both of these features have some correlation to the wall R-Value, but it is clear that neither could be a good predictor of the R-Value on its own.

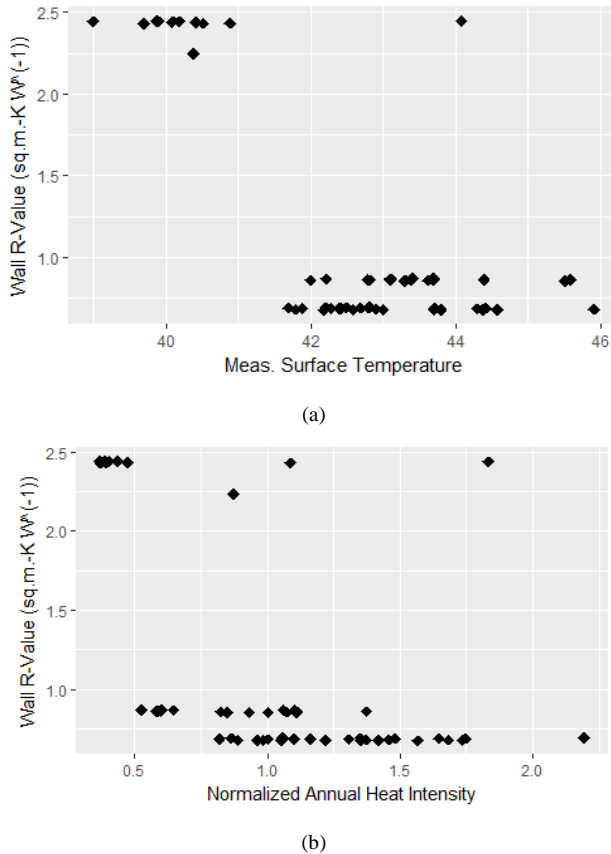


Figure 3: a). Measured wall temperature and b). Normalized annual heating consumption (NAHC) intensity versus measured wall R-Value for each of the 53 residences included in the study

Ultimately, the training data must include houses with low, medium, and high R-Values. The up-sampling method described in Sec. 3.2 is used for the training data in order to equalize the class data for wall R-Value. However, using an artificial test set for validation could lead to mischaracterization of model generality, and so instead the developed model is applied to the original dataset for verification.

D. Machine Learning Models and Validation

A number of machine learning models were explored and tested, including a random forest regression, a deep learning model, a support vector machine, and statistical model. We provide result detail for the two methods that performed the best, the random forest regression and the deep learning model. The random forest approach is an ensemble method that aggregates a series of individual regression trees (weak learners) in order to

reduce model variance, and which can readily incorporate complex, nonlinear feature interactions in order to predict a response. Random forest is an ensemble method that aggregates a series of weak learners (individual regression trees) in order to reduce model variance. Deep learning models connect input features to the output response through a series of nonlinear functions, and with sufficient data and network complexity have the capacity to encapsulate nearly any continuous functional form. Both methods have demonstrated reliable performance in building energy forecasting.

The loss function selected for both models was the mean squared error (MSE), defined as:

$$MSE = \frac{1}{n} \sum_{i=1}^n (y'_i - y_i)^2 \quad (5)$$

where n is the number of validation data points, y_i is the actual response variable, and y'_i is the predicted response.

The solution parameters used for each of the model techniques are as follows. For the deep learning model, a relatively simple architecture with 2 hidden layers, 12 nodes per layer, and a tanh activation function was selected as these model characteristics yielded the best prediction performance. For the random forest model, 500 trees and 3-5 decision variables for each tree were selected.

A randomized 10-fold cross-validation approach was used to develop and validate each of models using the original dataset. The samples were randomized, and split into 10 equal sections, or folds. One independent model was then constructed for each fold, using all data except that in the fold for training, and validating on the removed data in the fold. The errors from of each of these 10 validation sets were then averaged to give a final model score [31]. Two metrics are applied to establish the quality of the validation; namely the r-squared value and root mean square error. Further, given the limited number of observations included in the study (54), the randomized folds can affect the quality of the model. To eliminate any variation from the random fold selection, a large number of randomized folds were considered for each data grouping considered. The reported prediction test metrics are the averages of the individual prediction quality metrics for each randomized fold analysis.

III. RESULTS

The model validation performance demonstrated high accuracy. The RMSE for the scaled data (0-1) for the deep learning and random forest approaches were respectively 0.029 and 0.066. The r-squared values were similarly strong, equaling 0.995 and 0.978 respectively for the two techniques. We note that, given the clustering of responses towards the response extremes, r-squared values by themselves may provide an overly optimistic assessment of model performance. However, the combination of strong validation performance with respect to both RMSE and r-squared metrics is convincing. This is further evidenced by Figure 4, which shows the predicted versus actual scaled wall values for the complete up-sampled dataset for a) the deep learning approach and b) the random forest approach. The

jittered plots (whereby slight noise was added to the actual responses to slightly separate the points) show exceptional correspondence between predicted and observed values.

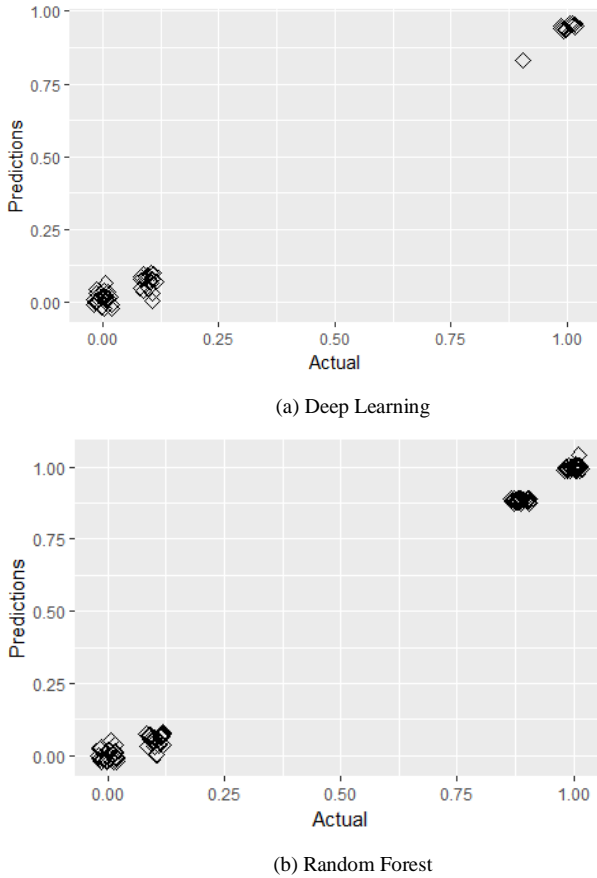


Figure 4: Predicted versus observed scaled wall R-Values for (a) deep-learning model and (b) random forest model. Note: points are shown with jitter for clarity.

In Table 4 we show the effect of inclusion of various features on the prediction quality. The various feature types are grouped by color, with light blue associated only with the thermography derived data, red corresponding to weather conditions at and just prior to the imaging, tan corresponding to energy characteristics derived from historical energy data, sky blue associated with geometrical data, and yellow corresponding to occupancy data. Both the RMSE and R-squared values are presented. The prediction quality for three general data groupings is shown, including IR + weather, derived energy characteristics + geometrical + occupancy, and all features.

When only the thermography-derived surface temperature is employed, the prediction quality is relatively poor (RMSE = 0.110, $R^2 = 0.901$). The addition of the outside temperature at the time of imaging improves the prediction quality improves sign (RMSE = 0.090, $R^2 = 0.910$). This RMSE suggests a mean error of 9% of the difference between the maximum and minimum R-Value. Inclusion of the weather conditions prior to the imaging time worsens the prediction quality.

We also explored use of only the derived energy characteristics, in conjunction with the geometrical and

occupancy data. The energy characteristics alone yield a better prediction quality than the coupling of IR and weather data (RMSE = 0.62, $R^2 = 0.973$). The addition of occupancy causes some decline in the prediction quality (RMSE = 0.62, $R^2 = 0.967$). These results cooperate findings by Altarhuni et al. who showed that derived energy characteristics and geometry data can be used to fairly accurately predict physical energy characteristics [12]. The last case considered within this grouping shows the effect of adding weather data to the derived energy characteristics, geometry, and occupancy on the prediction quality. The weather data at the time of the imaging should be irrelevant given the exclusion of the IR derived data. We observe a slight reduction in prediction quality, which would be expected when irrelevant data is added as features.

The fundamental question we were trying to answer is “can IR data be combined with derived energy characteristics, geometrical, and occupancy data to improve prediction of the wall R-Value?” The last data grouping presents prediction quality to answer this question. In general, the prediction quality is improved compared to the prior groupings. The best prediction quality is obtained when all of the data features are included (RMSE = 0.110, $R^2 = 0.901$). This represents about a 25% improvement in prediction accuracy relative to the prediction using derived energy characteristics and geometrical data alone, and an 80% improved accuracy relative to the prediction using IR derived and weather data.

Table 4: Prediction quality for variable input features

Data Grouping	Features											RMSE/ R2	
	IR	Weather						Derived Energy Char.s		Geom.	Occ		
	$T_{\text{transmired}}$	T_{out}	$T_{\text{out}-2}$	$T_{\text{out}-5}$	$T_{\text{out}-12}$	\bar{F}_{dir}	L_{dir}	HS	T_{dwb}	$E_{\text{residential, gas}}$	$A_{\text{ext}}/A_{\text{int}}$	O_{p}	
IR +	x												0.116/ 0.901
Weather	x	x											0.090/0.910
Energy Char.s/	x							x	x				0.128/0.890
Geom.	x										x		0.076/ 0.957
Occ	x											x	0.062/0.973
All	x	x	x	x	x	x	x	x	x	x	x	x	0.066/ 0.967
	x	x	x	x	x	x	x	x	x	x	x	x	0.067/ 0.965
	x	x	x	x	x	x	x	x	x	x	x	x	0.063/ 0.974
	x	x	x	x	x	x	x	x	x	x	x	x	0.058/ 0.975
	x	x	x	x	x	x	x	x	x	x	x	x	0.055/ 0.980
	x	x	x	x	x	x	x	x	x	x	x	x	0.054/ 0.979
	x	x	x	x	x	x	x	x	x	x	x	x	0.052/ 0.982
	x	x	x	x	x	x	x	x	x	x	x	x	0.050/ 0.982
	Key												
	x	IR Data				Weather Data		Derived Characteristics from Energy Data					
		Geometry Data				Occupancy Data							

It is important to note that the prediction quality shown in Table 4 represents the average prediction quality from 50 random folds for each data grouping considered. These average results do not change if a larger number of random folds are considered.

IV. CONCLUSIONS

The ability to perform energy audits of buildings at large scales and at low cost is essential for the rapid adoption of energy reduction strategies. Remote, automated thermal imaging to estimate envelope R-Values could be a component of this type of energy auditing. Our research demonstrates that machine learning can be used to accurately predict the wall R-value using only the IR derived exterior surface temperature measurement, weather conditions at and prior to the imaging time, derived residential energy characteristics from historical

metered energy data and weather data, geometrical data, and occupancy data.

There is still much research needed. First, there is a need to sample far more houses across a broad range of climate conditions to improve both the model performance and generality. Additionally, this study examined only residences with wood or plastic siding. Brick and stone walls are more massive than the walls considered here, and thus the dynamic weather effects will be different. It is almost certain that the training set of residences of known R-Values will need to grow to account for different types of walls. Lastly, the models developed here could be improved by leveraging smart WiFi thermostat data to document the temperature setpoint schedule(s) in the residence at and prior to the imaging time. The prediction accuracy would almost certainly be improved by including factors in the model that provide greater detail about the transient weather conditions prior to the imaging time.

There are numerous large-scale opportunities for this approach. Geo-referenced drive-by or drone-based fly-over thermal imaging is feasible. Thus the IR derived exterior temperatures could be automated and could be relatively low cost. For example, LiDAR GIS mapping, which has been highly automated, of the U.S. state of Indiana is estimated to cost on the order USD\$50/square kilometer [32]. If similar costs for automated thermal imaging could be realized, then in dense urban areas, which can have up to 8,000 homes per square km, the per home price of thermal imaging could be well less than USD\$1 per house.

In conclusion, our work helps to demonstrate the potential of merging IR derived exterior wall temperatures, historical energy data, weather data, building geometry data, and even occupancy data available for residences to automatically predict the wall R-Value. We anticipate that a similar methodology could be used to predict roof R-Values. More generally this work shows that it may be possible to simply leverage available information and readily collectable information to automatically audit the energy effectiveness of residences. If this could be achieved then energy efficiency programs could more strategically be designed to focus on investment of the most cost effective energy reduction opportunities for individual residences and among a group of residences.

V. REFERENCES

- [1] Michaels, "EIA U.S Energy Information Administration," 2015. [Online]. Available: <https://www.eia.gov/consumption/commercial/reports/>.
- [2] Waide, J. Amann and A. Hinge, "International Energy Agency," 2007. [Online]. Available: https://www.iea.org/publications/freepublications/publication/NAM_Building_Stock.pdf.
- [3] Hojjati, "Energy Information Administration," 2004. [Online]. Available: <https://www.eia.gov/consumption/archive/residential/insulation.pdf>. [Accessed 10 Nov. 2015].
- [4] Karaguzel and K. Lam, "Carnegie Mellon University," 2012. [Online]. Available: https://www.andrew.cmu.edu/user/okaraguz/TechnicalWritingSamples/Envelope_Parametric_01.pdf. [Accessed 25 January 2016].
- [5] Baechler, M. Strecker and J. Shafer, "Pacific Northwest National Laboratory," 2011. [Online]. Available: http://www.pnnl.gov/main/publications/external/technical_reports/PNNL-20956.pdf.
- [6] Stevie, "Integral Analytics," 1990. [Online]. Available: <http://www.integralanalytics.com/files/documents/Projecting%20Energy%20Efficiency%20Program%20Costs%202015.pdf>. [Accessed 11 Nov. 2013].
- [7] Adams, A. Miller and C. Higgins, "Deep Savings for Small Commercial Direct Install A Replicable Model for High Volume, Cost Effective Energy Savings," in 2016 ACEEE Summer Study on Energy Efficiency in Buildings, 2016.
- [8] Zhao and F. Magoulès, "A review on the prediction of building energy consumption," *Renewable and Sustainable Energy Reviews*, vol. 16, no. 2012, pp. 3586-3592, 2012.
- [9] P. Hallinan, P. Brodrick, J. Northridge, J. K. Kissock and R. Brecha, "Establishing Building Reconditioning Priorities and Potential Energy Savings from Utility Energy Data," *ASHRAE Transactions*, vol. 117, no. 2, p. 495, 2011.
- [10] Desogus, S. Mura and R. and Ricciu, "Comparing different approaches to in situ measurement of building components thermal resistance," *Energy and Buildings*, vol. 43, pp. 2613-2620, 2011.
- [11] Biddulph, V. Gori, C. Elweel, C. Scott, C. Rye and R. Lowe, "Inferring the thermal resistance and effective thermal mass of a wall using frequent temperature and heat flux measurements," *Energy and Buildings*, vol. 78, pp. 10-16, 2014.
- [12] Altarhuni, A. Naji, K. P. Hallinan and R. Brech, "Predicting Residential Heating Energy Consumption and Savings from Known Energy Characteristics and Historical Energy Consumption," in "Predicting Residential Heating Energy Consumption and Savings from Known Energy Characteristics and Historical Energy Consumption," in *Predicting Residential Heating Energy Consumption and Savings from Known Energy Characteristics and Historical Energy Consumption*, Atlanta, 2016.
- [13] Matheson, "MIT News," Massachusetts Institute of Technology, 2015. [Online]. Available: <http://news.mit.edu/2015/startup-essess-heat-mapping-cars-0105>. [Accessed 21 March 2016].
- [14] Ofukany, "PPP," GISUS 2010, 2010. [Online]. Available: <http://www.p3.sk/domain/flox/files/gis/8prezentacia-gisus-cedaslovakia-2008.pdf>. [Accessed 11 Nov. 2016].
- [15] Albatici and A. Tonelli, "On site evaluation of U-value of opaque building elements: a new methodology," in PLEA 2008 - 25th Conference on Passive and Low Energy Architecture, Dublin, Ireland, 2008.
- [16] Albatici and A. Tonelli, "Infrared thermovision technique for the assessment of thermal transmittance of opaque buildings elements on site," *Energy and Buildings*, vol. 42, p. 2177, 2010.
- [17] Albatici, A. Tonelli and M. Chiogna, "A comprehensive experimental approach for the validation of quantitative infrared thermography in the evaluation of building thermal transmittance," *Applied Energy*, vol. 141, pp. 218-228, 2015.
- [18] Grinzato, P. Bison, G. Cadelano and F. Peron, "R-value estimation by local thermographic analysis," *SPIE Defense, Security, and Sensing*, vol. 7661, no. 76610H, pp. 1-15, 2010.
- [19] Jardi, S. Sfarra and D. Ambrosini, "Quantitative thermography for the estimation of the U-value: state of the art and a case study," *J. of Physics: Conference Series*, vol. 547, pp. 1-8, 2014.
- [20] Jardi, D. Paoletti, D. Ambrosini, T. de Rubeis and S. Sfarra, "U-value assessment by infrared thermography: A comparison of different calculation methods in a Guarded Hot Box," *Energy and Buildings*, vol. 122, pp. 211-221, 2016.
- [21] Kokaides and S. Kalogirou, "Application of infrared thermography for the determination of the overall heat transfer coefficient (U-Value) in building envelopes," *Applied Energy*, vol. 88, pp. 4358-4365, 2011.
- [22] Y. Ham and M. Golparvar-Fard, "Automated cost analysis of energy loss in existing buildings through thermographic inspections AND CFD analysis," in *ISARC 2013 - 30th International Symposium on Automation and Robotics in Construction and Mining, Held in Conjunction with the 23rd World Mining Congress*, Montreal, QC, Canada, 2013.

- [23] Y. Ham and M. Golparvar-Fard, "3D Visualization of thermal resistance and condensation problems using infrared thermography for building energy diagnostics," *Visualization in Engineering*, vol. 2, pp. 12-26, 2014.
- [24] Y. Ham and M. Golparvar-Fard, "Mapping actual thermal properties to building elements in gbXML-based BIM for reliable building energy performance modeling," *Automation in Construction*, vol. 49, pp. 214-224, 2015.
- [25] G. Dall'O, L. Sarto and A. Panza, "Infrared Screening of Residential Buildings for Energy Audit Purposes: Results of a Field Test," *Energies*, vol. 6, pp. 3859-3878, 2013.
- [26] M. Fox, D. Coley, S. Goodhew and P. De Wilde, "Time-lapse thermography for building defect detection," *Energy and Buildings*, vol. 92, pp. 95-106, 2015.
- [27] R. Madding, "Finding R-values of stud frame constructed houses with IRthermography,," in *Inframation*, Reno, NV, U.S., 2008.
- [28] S. Alshatshati, K. Hallinan and R. Brecha, "Estimating Building Envelope Thermal Characteristics From Single-Point-in-Time Thermal Images," in *ASME 2016 International Mechanical Engineering Congress and Exposition*, Charlotte, 2016.
- [29] M. Bitterice, A. Lutz and W. R. Siskos, "windowanddoor," 2004. [Online]. Available: <https://windowanddoor.com/sites/windowanddoor.com/files/GlassEffects-Vinylcladding.pdf>. [Accessed 2 Jan 2017].
- [30] ThermoWorks, "Thermo Works," ThermoWorks, 2017. [Online]. Available: http://www.thermoworks.com/learning/emissivity_table. [Accessed 06 January 2017].
- [31] M. Stone, "Cross-validatory choice and assessment of statistical predictions," *J. of the Royal Statistical Society Series B (Methodological)*, vol. 36, no. 2, pp. 111-147, 1974.
- [32] State of Indiana, "Indiana Imagery Pricing Program," 2011. [Online]. Available: https://www.in.gov/gis/files/Ortho_-_Program_Pricing.pdf.